This document was prepared in conjunction with work accomplished under Contract No. DE-AC09-96SR18500 with the U.S. Department of Energy.

WSRC-STI-2007-00579

Permeability, Solubility and Diffusivity of Hydrogen Isotopes in Stainless Steels at High Gas Pressures

Edited by:

Chris San Marchi	(Sandia National Laboratories)
Brian Somerday	(Sandia National Laboratories)
Steve Robinson	(Sandia National Laboratories)

Contributors:

Chris San Marchi	(Sandia National Laboratories)
Brian Somerday	(Sandia National Laboratories)
Steve Robinson	(Sandia National Laboratories)
Mike Morgan	(Savannah River National Laboratory)
Karthik Subramanian	(Savannah River National Laboratory)
Phil Schembri	(Los Alamos National Laboratory)
Nick Wheeler	(Kansas City Plant)

Sandia National Laboratories
Livermore, CA

Publication date: September 12, 2005

I. INTRODUCTION

The aim of this report is to describe the framework necessary for extrapolating literature data for permeability, solubility, and diffusivity of hydrogen isotopes in stainless steels to conditions of high (>35 MPa) gas pressures. Experimental measurements are typically made under conditions of ideal gas behavior, however design of high-pressure hydrogen gas systems necessitates tools that incorporate real gas behavior. In addition, we want to address inconsistencies in data and make specific recommendations for permeability, solubility, and diffusivity relationships for the temperature range near ambient and high pressure. As will be shown below, deviations from ideal gas behavior are important when extrapolating low pressure "ideal gas" experiments to engineering analysis of real high-pressure systems. Permeability data is derived at low pressure where ideal gas behavior is a valid assumption, however at pressures of engineering interest for hydrogen storage, on the order of 100 MPa, deviations from ideal behavior can be large.

II. BACKGROUND

2.1 Equation of State: Gases

The equation of state describes the thermodynamic state of a system and for gases this requires knowledge of two variables such as the pressure and temperature of the system. Ideal gases are described by a simple relationship:

$$V_m^o = RT/P \tag{1}$$

where V_m^o is the molar volume of the ideal gas, P and T are the absolute pressure and absolute temperature of the system respectively, and R is the universal gas constant equal to 8.31434 J mol^{-1} K^{-1}. Real gas behavior is often characterized by the compressibility factor $Z = PV_m/RT$, where V_m is the molar volume of the real gas. The compressibility factor is one for the ideal gas and generally shows a positive deviation ($Z > 1$) at high pressure.

From basic thermodynamic relationships, the chemical potential of any system can be expressed as:

$$\left(\frac{d\mu}{dP}\right)_T = V_m \tag{2}$$

For an ideal gas, this relationship can also be written in the form

$$(d\mu)_T = RT(d\ln P)_T. \tag{3}$$

This is the familiar form of the chemical potential where the pressure can be thought of as the "activity" of the ideal gas. It should be noted also that the pressure term has no units since it represents dP/P.

Deviations from ideal behavior are important due to the finite volume of the gas and electronic interactions between the molecules for example. This is particularly apparent at high pressure and low temperature, thus the fugacity *f* is introduced. The form of the fugacity is chosen for convenience to have a form analogous to that of the ideal case, that is

$$(d\mu)_T = RT(d\ln f)_T \tag{4}$$

Fugacity is often described as an effective pressure or as the activity of the real gas. It is generally assumed that all gases behave ideally at infinitely low pressure, therefore as $P \to 0$ then $f \to P$. With knowledge of the fugacity the thermodynamics of real gases can be rigorously treated. By combining equations 1–4 and integrating, the fugacity can be related to the equation of state and the properties of the ideal gas

$$\ln\left(f/f_o\right) - \ln\left(P/P_o\right) = \frac{1}{RT}\int_{P_o}^{P}\left(V_m - V_m^o\right)dP \tag{5}$$

where f_o and P_o are the fugacity and pressure respectively at some reference pressure. Using the limiting behavior of fugacity $(f_o \to P_o \to 0)$ and the equation of state for an ideal gas, equation 1, the fugacity can be expressed in the form

$$\ln\left(\frac{f}{P}\right) = \int_0^P\left(\frac{V_m}{RT} - \frac{1}{P}\right)dP \tag{6}$$

Equation 6 is the fundamental relationship between the equation of state and the fugacity, which is sometimes referred to as the definition of fugacity. Theoretically, *f* has no units, but it must be expressed in the same units as pressure since $f_o \to P_o$, therefore it is convenient to attach pressure units to fugacity.

There are numerous models and empirical relationships that account for the nonideal behavior of gases, however these are often complicated transcendental equations that cannot be easily manipulated analytically [1-5]. The Abel-Noble equation of state, on the other hand, is a single parameter relationship of the form

$$V_m = \frac{RT}{P} + b \tag{7}$$

where *b* is a constant. The simplicity of this relationship is notable when compared to other equations of states for real gases, such as virial equations, which may include upwards of ten parameters, many of which are themselves functions of temperature [1-3]. At pressures of general engineering significance (< 200 MPa) and temperatures near ambient the Abel-Noble equation tracks the compressibility factor,

$$Z = 1 + Pb/RT \tag{8}$$

of a number of real gases to better than a few percent [6]. Other equations of state can better fit real gas behavior by empirically fitting data with additional parameters, although in the literature equations of state are fit to data over a wider range of pressure, but sacrificing correlation at relevant engineering pressure [1-4].

Substituting the Abel-Noble equation of state, equation 7, into the "definition" of fugacity, equation 6, the fugacity can be expressed as a simple function of pressure and temperature:

$$f = P\exp\left(\frac{Pb}{RT}\right) \tag{9}$$

The ratio of the fugacity to the pressure is often called the fugacity coefficient. This simple closed form of the fugacity allows for analytical determination of thermodynamically dependent phenomena such as permeability and solubility while accurately incorporating the real behavior of the gas phase. This is particularly useful for treating the thermodynamics of high-pressure gaseous systems, since extrapolating low pressure "ideal gas" experiments to engineering analysis of real high-pressure systems requires understanding the nonideal behavior of real gases.

2.2 Solubility

In this section, we develop the relationship for solubility *K* assuming equilibrium between the diatomic hydrogen molecule and hydrogen atoms in the material:

$$\tfrac{1}{2}\mathrm{H}_2 \Leftrightarrow \underline{\mathrm{H}} \tag{10}$$

Although we assume hydrogen in this analysis, these relationships are general for any diatomic gas, including isotopes of hydrogen. At equilibrium, the chemical potential of the gas must be equivalent to the chemical potential of dissolved hydrogen in the material: $\tfrac{1}{2}\mu_{\mathrm{H}_2} = \mu_{\underline{\mathrm{H}}}$. We assume that atomic hydrogen dissolved in the material behaves as a dilute solution (Henrian standard state), and that the nonideal behavior of the hydrogen gas must be considered, therefore

$$\tfrac{1}{2}\left(\mu^o_{\mathrm{H}_2} + RT\ln f\right) = \mu^o_{\underline{\mathrm{H}}} + RT\ln\chi \tag{11}$$

where χ is the equilibrium concentration of hydrogen dissolved in the metal, the superscript *o* refers to the standard state. The difference in chemical potential between the standard states is related to the heat of solution of hydrogen atoms ΔH_s and the entropy ΔS_s:

$$\left(\mu^o_{\underline{\mathrm{H}}} - \tfrac{1}{2}\mu^o_{\mathrm{H}_2}\right) = \Delta H_s - T\Delta S_s \tag{12}$$

Combining equations 11 and 12 the concentration of dissolved hydrogen in equilibrium with the hydrogen gas can be expressed as

$$\chi = Kf^{1/2} \tag{13}$$

where

$$K = K_o \exp\left(-\Delta H_s / RT\right) \tag{14}$$

Equation 13 can also be written directly by following basic procedures for expressing chemical equilibrium of the reaction shown in equation 10, where *K* is the equilibrium coefficient. This relationship is equivalent to Sievert's Law in the limit of ideal gas behavior ($f \to P$) in which case *K* is the so-called Sievert's parameter. Sievert's Law is a special case of chemical equilibrium in the limit of ideal gas behavior, while equation 13 is the more general form.

Equation 13 relates the equilibrium concentration of atoms from a diatomic gas in a metal χ to the fugacity (pressure) of this diatomic gas *f*. It is important to make the distinction between solubility and concentration: the solubility *K* of a species from a gas is independent of the fugacity (pressure) but a function of temperature (equation 14), while the concentration χ depends on the fugacity (pressure) as in equation 13 and temperature. Often in the literature the term solubility is incorrectly used to refer to concentration. Solubility of a gas in a solid should always have a pressure unit associated with it.

Data fit to this Arrhenius relationship for solubility is commonly reported in the literature for materials exposed to hydrogen gas and its isotopes: deuterium and tritium. Care must be extended in comparing data from the literature as in some cases the heat of solution may be reported per mole of hydrogen gas ($H_2 \Leftrightarrow 2\underline{H}$), which requires a factor of two to be expressed in the denominator of exponential term in equation 11 [7].

2.3 Diffusion and Permeability

Permeability of hydrogen and its isotopes is generally defined as the steady state diffusional transport of atoms through a material that supports a pressure difference. Assuming steady state, an infinite plate, and Fick's first law for diffusion $J = -D(dc/dx)$, we can write

$$J_\infty = D\frac{(\chi_t - \chi_0)}{t} \tag{15}$$

where J_∞ is the steady state diffusional flux, *D* is the diffusivity, χ is the concentration just under the surface on either side of the plate and *t* is the thickness of the plate. Using chemical equilibrium (equation 13) for nonideal gas and assuming that the hydrogen partial pressure is negligible on one side of the plate, the diffusional flux can be expressed as

$$J_\infty = \frac{DK}{t} f^{1/2} \tag{16}$$

where the product *DK* is defined as the permeability Φ. Equation 16 is sometimes called Richardson's Law. There are numerous conditions under which this relationship may not be valid (under very high vacuum, at very high pressure or temperature; see Ref. [8] for an

extensive discussion of permeation); however, under most engineering conditions, this relationship is well established [9].

The majority of studies on permeation use a direct measurement technique to determine the flux of hydrogen or deuterium permeating through a membrane or disk of the material of interest. In one manifestation of this technique, a constant pressure of hydrogen (or deuterium) is maintained on one side of the membrane and a vacuum on the other side. The rate of hydrogen escape on the vacuum side of the membrane is measured at steady state with a leak detector or other suitable method. Diffusivity in the membrane material is determined by analyzing flux transients and back calculating a diffusion coefficient from solutions to the flux equation [10].

Both permeability and diffusivity are thermally activated processes, thus they feature an Arrhenius-type dependence on temperature and, like solubility, they can be expressed in the general form:

$$\Phi = \Phi_o \exp\left(-H_\Phi \big/ RT\right) \tag{17}$$

$$D = D_o \exp\left(-H_D \big/ RT\right) \tag{18}$$

respectively.

Since $\Phi \equiv DK$, solubility is determined from the ratio of the direct measurements of permeability and diffusivity as

$$K = \frac{\Phi_o}{D_o} \exp\left[-\left(H_\Phi - H_D\right) \big/ RT\right] \tag{19}$$

The solubility can be thought of as the pressure-normalized equilibrium concentration of hydrogen within the metal crystal lattice. This method for determining permeability, diffusivity and solubility assumes that hydrogen transport is governed by diffusion in the bulk; therefore, care must be taken to ensure that surface chemistry or other phenomena do not intervene as rate limiting processes.

Hydrogen concentrations measured by other techniques such as hydrogen extraction are also commonly referred to as solubilities. In general, however, these measurements do not represent the lattice hydrogen that drives diffusion. In many materials, hydrogen can be trapped at microstructural features (e.g., point defects, line defects, and surface defects) and does not contribute to the transport of hydrogen across the membrane. Hydrogen extraction measures the total concentration of hydrogen, which is the sum of trapped and lattice hydrogen. Therefore, hydrogen concentrations determined by techniques that do not distinguish between hydrogen that diffuses through the lattice and hydrogen trapped in the microstructure should not be used to determine solubility; rather the term solubility should be reserved for a measure of lattice hydrogen. Incidentally, being related to the lattice, the solubility (as well as permeability and diffusivity) should be viewed as a physical property of the material and, to a first order

approximation, should be independent of microstructure. Like all physical properties, however, these properties can be dependent on composition.

2.4 Mass/Isotope effects

It is commonly assumed that the ratio of diffusivity of hydrogen isotopes is equivalent to the inverse ratio of the square root of the masses of the isotopes:

$$\frac{D_H}{D_D} = \sqrt{\frac{m_D}{m_H}} \tag{20}$$

where D and m are the diffusivity and mass of the respective isotope, and the subscripts H, D, and T refer to hydrogen, deuterium and tritium respectively. Similar expressions can be written for tritium and can be simplified as $D_H = \sqrt{2}D_D = \sqrt{3}D_T$. These relationships between isotopes stem from classical rate theory, which relates diffusivity to atomic vibrational frequencies and these frequencies are inversely proportional to mass. The activation energy for diffusion is also assumed to be independent of the mass of the isotope. Diffusion data at subambient temperatures do not support equation 20 for a number of metals [11], however, permeability data at elevated temperatures generally support the inverse square root dependence on mass for nickel [12] and stainless steels [13-16]. For the purposes of this report we assume that equation 20 is a good approximation for both permeability and diffusivity; implicitly then the solubility is assumed to be independent of the mass of the isotope.

III. DISCUSSION

3.1 Equation of state: hydrogen and its isotopes

Assuming that the Abel-Noble equation of state provides a good prediction for hydrogen and its isotopes, the compressibility factor should be a linear function of pressure (equation 8). McLennan and Gray [3] plot data for hydrogen and deuterium from Michels at al., which indeed appear linear for temperatures in the range of 273 K to 423 K, and for pressures from ambient to 200 MPa, i.e. high pressures of engineering relevance. As part of this work, all of the hydrogen data of Michels et al. [17] for temperature ≥ 273 K was fit to the Abel-Noble form of the equation of state. The constant b was determined to be 15.55 $cm^3\ mol^{-1}$ for hydrogen in good agreement with the report of Chenoweth for deuterium [6]. The compressibility factor from measured data Z_{meas} is plotted in Figure 1 as a function of hydrogen pressure and temperature for data from Michels et al. [17] and Vargaftik [18]. The lines in Figure 1 represent the calculated compressibility factor Z_{calc} for the given temperature from equation 8 with b = 15.55 cm^3/mol. Figure 2 shows a plot of the ratio of the calculated to measured compressibility factor (Z_{calc}/Z_{meas}) for data of Michels et al. [17] and Vargaftik [18], showing that the Abel-Noble equation of state provides a good representation of real hydrogen gas behavior in the temperature range from 273 K to 423 K for pressure ≤ 200 MPa, as well as at elevated temperature, although for somewhat lower pressure. There is data to support this equation of state to pressures as high as 100 MPa at temperature of 800 K and for pressure up to 50 MPa at temperature of 1000 K.

For all of the plotted data the calculated values of *Z* are within 1.2% of the measured values and generally within a fraction of a percent of the measured values of *Z*.

The range of applicability quoted above for elevated temperature are limited by the available data, however, based on trends for real gases, it is expected that the Abel-Noble equation of state with *b* equal to 15.55 $cm^3\ mol^{-1}$ can be applied to significantly higher pressures at elevated temperature, probably as high as 200 MPa for temperature from ambient to 1000 K. A relatively large divergence of Z_{calc}/Z_{meas} was noted for pressure >250 MPa at near ambient temperature; thus an upper bound on pressure of 200 MPa was chosen for fitting the Abel-Noble equation of state. No attempt was made to fit data at low temperature (< 273 K) or to quantify the Abel-Noble relationship at these low temperatures. It is, however, clear from the plots of McLennan and Gray [3] that *Z* begins to diverge from linearity at subambient temperature.

The constant *b* is expected to be appropriate for deuterium and tritium as well. Indeed, the value of 15.55 cm^3/mol determined here is in good agreement with the report of Chenoweth for deuterium [6]: Chenoweth reports a value of 15.5 cm^3/mol, which was determined using the data of Michels et al. [17]. McLennan and Gray plot the data of Michels et al. for hydrogen and deuterium [3] showing that the compressibility of these gases is essentially the same for most conditions (for temperatures in the range of 273 K to 423 K and pressures from ambient to 200 MPa). Differences in compressibility between hydrogen and deuterium decrease as temperature is increased, but increase with pressure. For pressures of engineering relevance (< 200 MPa), however, the differences between hydrogen and deuterium are small for temperatures ≥ 273K; divergence between the compressibility fractors of hydrogen and deuterium is apparent at lower temperature [3]. The Abel-Noble equation of state with $b = 15.5\ cm^3$/mol is expected to provide a good estimate of real behavior of tritium gas (as well as hydrogen and deuterium) over these same pressure and temperature ranges.

3.2 Effect of Pressure and Temperature

Experimentally, temperature and pressure are varied in permeability studies over some range to determine the Arrhenius temperature dependence and confirm the square root dependence of fugacity as predicted by chemical equilibrium (square root dependence of pressure, i.e., Sievert's law, for the special case of an ideal gas). The square root dependence on fugacity is often assumed, however. Under some conditions, such as low pressure (on the order of 10 Pa) or specific surface chemistry, the square root dependence on fugacity has been found to be inappropriate [8] [19], thus studies at low pressure or without careful consideration of the exposed surfaces should be viewed critically. It has been shown that permeability data can be extrapolated with confidence to at least a pressure of 25 MPa for nickel [12], and solubility data to a pressure of 50 MPa at 773K for stainless steel [20]. Permeation at higher pressures has not been confirmed.

In general, permeability studies are performed at temperatures and pressures significantly different from conditions relevant to gaseous hydrogen distribution and storage in engineering applications. Tests are typically performed at pressures near ambient (or lower) and temperatures greater than 200˚C, while pressurized systems for the storage of gaseous hydrogen operate near

ambient temperature and at pressures potentially up to 138 MPa. The experimental conditions are necessitated by the desire to make measurements in a safe and efficient manner, thus low pressure and high temperature respectively. The measured relationships are then extrapolated to the engineering conditions of interest. Nevertheless, the mechanisms of lattice transport are not expected to change in these ranges of temperature and pressure; additionally, the square root dependence of fugacity on hydrogen transport is expected to be a good approximation for all pressures above ambient and temperatures where thermal dissociation of hydrogen can be neglected, i.e., temperature less than about 1273K [8].

As shown from first principles, the fugacity should be rigorously applied in solubility and permeability rate calculations, but this has only rarely been acknowledged in the literature in the context of hydrogen effects on material properties [21-23]. The real gas behavior of hydrogen (and its isotopes) becomes apparent in the fugacity function at modest pressures and ambient temperature, although real gases tend toward ideal behavior (fugacity tends toward the pressure) as temperature is increased. Thus at elevated temperatures and relatively low pressures ideal behavior is a good engineering approximation and for this reason, most studies on permeability and solubility have not accounted for fugacity. For pressures as low as 15 MPa at ambient temperature, however, the fugacity is about 10% greater than pressure. In terms of permeability and solubility it is the square root of this value that is relevant, which implies a rather modest correction for real gas behavior near ambient temperature and pressure < 15 MPa. Consequently, while it is not surprising that the real gas behavior of hydrogen has not been addressed in permeability and solubility studies, when extrapolating these studies to high-pressure gaseous hydrogen, the fugacity must be considered. At 273 K and a pressure of 200 MPa, for example, the fugacity is almost four times the pressure. For a comparatively modest pressure of 35 MPa (~5000 psi) the fugacity-pressure ratio is 1.25 at 298 K and the square root of this ratio is 1.12. The fugacity of hydrogen is plotted in Figure 3 as a function of pressure for several temperatures and assuming the Abel-Noble equation of state with b equal to 15.55 $cm^3\ mol^{-1}$.

3.3 Oxidation and Surface Effects

By definition, permeability and solubility are independent of surface condition as these parameters are defined in terms of diffusion of hydrogen through the lattice. In practice, however, experimental measurements are strongly influenced by surface condition. Oxides have been proposed as diffusion barriers for austenitic stainless steels in first wall fusion reactors [24, 25]. These oxides, in some cases, have been shown to significantly reduce the apparent permeability [14, 26]. When these oxides are very thin, the oxide is thought to reduce the kinetics of hydrogen dissociation on the surface creating a process that is not rate controlled by diffusion and thus not a true permeability. The permeability of oxidized stainless steel was recovered in one study by coating with palladium after oxidation [14]. The palladium catalyzes the dissociation of hydrogen eliminating this kinetic barrier and establishing conditions of diffusion-controlled transport of hydrogen. The implication of this observation is that the diffusivity through the oxide is similar to that in the metal. One the other hand, the permeability is relatively unaffected by thick oxides; the interpretation being that once the oxide layer reaches a critical thickness the layers crack exposing metal surface [14, 25, 26]. It should be emphasized as well that when surface conditions modify the kinetics of hydrogen transport, the square root

dependence of pressure is often lost [14, 26]. Very low pressure (< 10 Pa) also precludes the square root dependence on pressure and diffusion-controlled transport [9].

While oxides and surface films have been reported to reduce the apparent permeability in some metals, it should not be assumed that these surface conditions would persist under different environmental conditions. Most permeability tests are conducted at pressure on the order of 1 kPa, while the significantly higher fugacity of hydrogen at 100 MPa for example may result in reduction of the oxide and loss of the barrier effect [25, 26]. Moreover, the apparent changes in hydrogen transport appear to be the result of changing the rate-controlling step from lattice diffusion to some surface chemistry such as adsorption and dissociation, thus surface layers do not change the intrinsic hydrogen permeability of the material.

Oxides and surface films may not have a strong effect on steady-state hydrogen transport, in some cases [26], but may presumably have a substantial effect on hydrogen transport transients and thus diffusivity determinations. In addition, the diffusivity determination will be significantly affected by the specific method of determination, that is whether the flux transients are used to fit solutions to the diffusion equations, or whether a single characteristic time is used to calculate a diffusion coefficient. The former method offers some intrinsic averaging of the signal over a range of fluxes, while the latter method is susceptible to signal noise. In either case, these transients are likely to be more sensitive to surface conditions than the steady-state permeability determination.

A number of studies on austenitic stainless steels have attempted to correlate solubility with surface finish and resulting hydrogen embrittlement phenomena [27, 28]. As described above, the surface condition by definition cannot affect the solubility of the lattice material, since solubility assumes thermodynamic equilibrium between the lattice and the gas phase. The condition of the surface can, however, affect the kinetics of surface reactions, which will affect the establishment of equilibrium in the lattice. In addition, plastically deformed surfaces (e.g., by machining) can induce phase changes in some alloys (martensite in 304 stainless steel, for example, and η-phase in A-286), which will affect the surface kinetics as well as equilibrium.

In summary, the surface condition can have a profound impact on the measured quantities in permeation studies. The nomenclature established in any given study should be carefully considered before interpreting and using results. For values that are true materials properties, the pressure dependence should be established and the surface chemistry should be controlled such that the process of hydrogen transport is indeed controlled by lattice diffusion.

3.4 Effect of Microstructure and Hydrogen Trapping on Transport

Hydrogen can be trapped at numerous microstructural features including grain boundaries, phase boundaries, second phases such as hydrides, and dislocations [10, 23]. Trap sites are generally categorized by the thermal energy required to remove the hydrogen atom from the trapping site, e.g., "weak" or "strong" traps. The concentration of hydrogen in traps is dictated by the trap binding energy, number of trapping sites, and temperature.

Several studies on austenitic steels have shown that hydrogen transport and solubility are independent of whether the microstructure is annealed or heavily cold-worked [27-29], as should be expected if dislocations are weak traps and the lattice solubility is high. There are occasions, however, when hydrogen transport and solubility may appear to depend on the microstructure of the alloy. Steel phases with a body-centered cubic (BCC) crystal structure, such as ferrite and martensite, have significantly higher hydrogen diffusivity and substantially lower hydrogen solubility than the face-centered cubic (FCC) austenitic phase. In relatively unstable austenitic stainless steel such as 304, cold-work can induce martensitic phase transformations, which then cause the effective transport properties, as well as solubility, to be substantially different from an annealed 304 stainless steel that is free of martensite [30, 31]. Ferrite is also common in austenitic stainless steels, particularly in high-chromium 300-series, and can have a significant effect on hydrogen transport properties if the ferrite is highly oriented, as in long thin stringers, or in high enough concentrations, as for duplex alloys. With the exception of conditions where second phases are present, solubility determined from permeability measurements and from hydrogen extraction techniques should provide similar results in austenitic stainless steels, since they are characterized by weak hydrogen trapping and high lattice solubility.

In contrast to austenitic stainless steels, strong traps and low lattice solubility characterize plain carbon and low alloy steels (indeed any steels with a BCC crystal structure). The measurement technique (e.g. permeation or gas analysis), as well as the hydrogen trapping characteristics of the microstructure and density of the traps, will strongly influence the apparent hydrogen concentration. It is important to consider the measurement technique when considering the hydrogen concentration in these alloys, and to use the value relevant to the phenomenon of interest. For example, for diffusive related processes the solubility is of interest, while in studies of hydrogen embrittlement the total hydrogen concentration or trapped hydrogen concentration determined by hydrogen extraction could perhaps be of more interest.

3.5 Permeability

LeClaire reviewed permeability data [9] and found that the majority of data for stainless steels is within factors of 1.5 and 1.5^{-1} of an average curve. Given that permeability changes of six orders of magnitude are predicted between ambient temperature and 673 K, the coincidence of permeability data for many austenitic alloys from many studies is rather remarkable, especially considering surface effects as described above. Other reviews of data on stainless steels [7] found similar consensus on permeability data (although the units quoted in Ref. [7] are believed to be incorrect, see appendix). Arrhenius relationships with the lowest activation energy terms

are recommended for use for two reasons: (1) as discussed by Louthan and Derrick [27], hydrogen transport through a material is affected by the surface condition, however, the activation energy should approach a minimum in the limit that permeation is purely governed by lattice diffusion through the bulk; and (2) lower activation energy leads to higher extrapolated permeability at ambient temperature, thus providing an upper bound to the permeation rate a low extrapolated temperature.

Average permeability relationships determined in studies that considered several austenitic alloys are summarized in Table 1. The permeability relationship of Louthan and Derrick [27], marked by circles in Figure 4, appears to be a good average relationship for austenitic stainless steels, particularly since it was generated from data of several alloys in both annealed and cold-worked conditions; three of the alloys were variants of type 304 stainless steel. The Louthan-Derrick relationship is for deuterium, but it has been corrected here for hydrogen by multiplying by $\sqrt{2}$. The average relationship of Sun et al. was also generated from six alloys in several conditions (solutionized, annealed and cold-worked) [29] and is marked with triangles in Figure 4. The other lines represent permeability determined for type 316 stainless steels from a number of studies [15, 16, 32-36].

For the unstable austenitic stainless alloys, such as 304 and 321, strain-induced martensite may form during thermomechanical processing or by deformation at low temperature [30, 31]. Martensitic phases have permeability and diffusivity several orders of magnitude greater than the austenitic phases. It has been observed that the presence of martensitic phases in austenitic stainless steel, for example as a consequence of cold-working the alloy, will greatly increase the permeability and diffusivity of hydrogen in the alloy [30, 31]. Cold-working stable austenitic alloys, such as 316 and 310 stainless steels, however, does not significantly affect the rate of hydrogen transport [29, 31].

3.6 Diffusivity

Measured values of hydrogen diffusivity in austenitic stainless steels are somewhat less consistent than permeability: Figure 5 shows the hydrogen diffusivity relationships for several 316 stainless steels determined from permeation studies (hydrogen permeability for these same studies are plotted in Figure 4, although not all studies that report permeability also report diffusivity). While permeability is commonly determined from a steady-state condition and thus can be time-averaged, diffusivity requires analysis of transient data and this leads to larger intrinsic uncertainty in the determination. Additionally, transient data are likely to be more sensitive to surface condition adding further uncertainty, as described above. These considerations explain the large scatter in diffusivity data, which is translated to solubility data, since solubility is determined from the ratio of permeability to diffusivity.

Studies that report the highest diffusivity share a common feature: special precautions were not taken to remove surface oxides or films. The relationships from these studies [15, 34, 35] are plotted as dotted lines in Figures 5 and 6. High diffusivity implies low solubility ($K = \Phi/D$), and since diffusivity and permeability are similar in magnitude over a wide range of temperature, small differences in diffusivity appear as large relative differences in solubility, Figure 6. The

relative solubility then provides a indirect indication of the accuracy of the diffusion determination. If we neglect the studies that result in low solubility [15, 34, 35] and only consider the studies where the solubility determinations cluster at the highest values [29, 32, 36], the hydrogen diffusivity relationships are in good accord with one another. The relationship of Louthan and Derrick [27], Table 1 and marked by circles in Figure 5, appears to represent a good average of diffusivity for austenitic stainless steels.

Variables that have second order effects on permeability determinations, such as alloy composition and perhaps microstructure, appear to have a greater effect on diffusivity. Sun et al., for example, noted that the hydrogen permeability of six austenitic stainless steel alloys were nearly indistinguishable, however, the alloys clustered into two groups with respect to hydrogen diffusivity [29]. Similar trends can be observed from other studies. For austenitic alloys it appears that hydrogen diffusivity may scale with the inverse of the chromium content, although the trend is certainly not a simple function of chromium only as discussed in the following section. Hydrogen diffusivity relationships that distinguish between specific austenitic alloys, such as 300-series stainless steels and the Cr-Ni-high Mn stainless steels, are discussed in the following section, since they are determined based on differences in hydrogen solubility. The role of second phases is also important, especially when those phases change crystal structure as BCC (ferritic) transformations in a FCC (austenitic) matrix, and can markedly change the apparent diffusivity as described above.

3.7 Solubility

Hydrogen solubility determined from permeation studies depends on the quality of the hydrogen diffusivity determinations, which can be compromised by inattention to surface kinetics and appropriate treatment of diffusion transients. For example, hydrogen diffusivity of type 316 stainless steel determined from a number of studies show significant inconsistency, Figure 6. A number of studies cluster near some upper bound in hydrogen solubility, while low values are scattered and generally have a steeper slope (higher heat of solution). The low solubility determinations correspond to high diffusion measurements, and are suspect as described in the previous section. As with permeability and diffusivity, the solubility relationship established by Louthan and Derrick provides a good estimation that appears to be conservative (high) at low temperature (Louthan and Derrick used deuterium in their study).

While the solubility at high temperature is certainly of interest, for many engineering applications the solubility at ambient temperature is of more concern. As the extrapolations in Figure 7 show for the data clustered at high solubility, the heat of solution (slope of the Arrhenius plot), has a strong impact on the extrapolated solubility. For studies that measured approximately the same solubility, the difference in heat of solution causes values extrapolated to ambient temperature to differ by an order of magnitude. The relationship with the lowest heat of solution will provide an upper bound on the extrapolated solubility and provide an upper bound to the amount of hydrogen present in the material. In addition, as described above, the theoretical minimum in the energy terms should be approached as surface effects are reduced, providing a scientific basis for choosing relationships with the lowest energy terms, such as that proposed by Louthan and Derrick for austenitic stainless steels [37].

The relationships of Louthan and Derrick, however, have been criticized for averaging the data for several austenitic alloys. Other evidence in the literature suggests that the solubility of 304 stainless steel is significantly less than 21Cr-6Ni-9Mn (21-6-9) [29]. Hydrogen concentration data from hydrogen extraction measurements of Caskey (Table 2) and within our own laboratory (Tables 3–7) also support the observation that the solubility of hydrogen in 21-6-9 and 22Cr-13Ni-5Mn (22-13-5) is greater than in 304 and 316 stainless steels for the same pressure and temperature, Figure 8. Caskey proposes two solubility relationships based on hydrogen extraction data and fitting tritium diffusion profiles to solubility and diffusion relationships. However, Caskey's solutions are not unique and no clear justification for the choice of energy terms is given. These relationships distinguish between 304 and 21-6-9 well enough but do not capture all of his own data. The deuterium data of Caskey, in particular, appears to be consistently low [20] and is not considered further here. In addition, the relationships generated by Caskey do not take into account real gas behavior, i.e., the fugacity. We have taken the hydrogen concentration data reported by Caskey (Table 2) in Refs. [20, 28] as well as our own data (Table 3 & 5) and used the lowest energy term (5.9 kJ mol^{-1}, Ref. [27]) along with the fugacity function determined in previous sections to generate solubility relationships for 304 and 21-6-9 respectively. The quantities for the hydrogen solubility relationships that have been determined here are give in both Table 1 and Table 8, as well as plotted in Figure 8 with average values for solubility for a number of austenitic alloys determined from hydrogen extraction data (from Tables 2–7). In addition, the differences in hydrogen diffusivity for these two alloys can be estimated by dividing the permeability (as measured from Louthan and Derrick for example) by these solubility relationships. The diffusivity for 304 and 21-6-9 as determined by this procedure are given in Table 8.

The lower heat of solution term determined by Louthan and Derrick, compared to Caskey and others, represents a lower limit and is believed to be the most appropriate value for austenitic stainless steels; in addition, from the view of extrapolation it represents an upper bound on hydrogen concentrations. Considering that the data represents two laboratories and in our case numerous hydrogen saturation trials, the fit is satisfying. The major assumption in constructing these relationships is that trapping can be neglected for austenitic stainless steels, such that the solubility can be approximated by hydrogen extraction data. The construction of alloy specific solubility relationships is motivated by the desire to express the hydrogen solubility as a function of temperature (between ambient and a few hundred degrees centigrade) to within 10 to 20%, compared to diffusivity and permeability, where a factor of two is generally sufficient since these values vary by many orders of magnitude over narrow temperature ranges.

Data for 316 and 22-13-5 stainless steels were not used to construct these improved solubility relationships but follow the predictions for 304 and 21-6-9 respectively. This adds further weight to these relationships as data from both permeation experiments (for hydrogen diffusivity) and hydrogen extraction studies indicate that the austenitic alloys seem to cluster into two groups [29]. The precipitation-strengthened austenitic stainless steels (A-286 and JBK-75, which are treated as a single alloy for this analysis due to the relatively small amount of data) appear to show a different solubility depending on whether the alloy is annealed or aged. In the annealed condition a "modified A-286" [28] (presumably JBK-75) was found to have a hydrogen concentration similar to 304L, while in the forged condition (and presumably aged) the alloy

features a significantly lower hydrogen concentration. Our own measurements on peak aged A-286 and JBK-75 alloys (Table 7) also show a lower hydrogen concentration than measured for 304L (Table 3) and 316L (Table 4) under the same conditions. Thus, data for the precipitation-strengthened austenitic alloys are used to determine a solubility relationship and a diffusivity relationship (Table 8) in the same manner as described above for 304L and 21-6-9. Permeability studies on JBK-75, however, have shown very little effect of aging on hydrogen diffusivity in this alloy, although hydrogen permeability appears to be slightly higher in the solution heat treated condition, which translates to a higher hydrogen solubility in the solution heat treated condition [38].

Alloy composition is generally believed to be the source for differences in between the 300-series and the nitrogen-strengthened alloys. Nitrogen as well as high manganese and high chromium have been implicated since these are distinguishing characteristics of 21-6-9, 21-9-9 and 22-13-5 all of which appear to have significantly higher solubility than the 300-series alloys. Nitrogen-strengthened 300-series alloys, 316N and 304LN, however do not display higher solubility than their counterparts without nitrogen [27, 29]. High chromium and manganese may explain some alloys, but type 321 stainless steel has high solubility and relatively low chromium and manganese (and no nitrogen). Titanium has been implicated to explain type 321 stainless steel. This does not explain, however, the relatively low solubility of hydrogen in A-286 and JBK-75 (Figure 8) as these alloys have among the highest chromium, nickel and titanium contents of all the alloys that have been discussed. Further study is necessary to clarify these ideas.

IV. RECOMMENDATIONS AND CONCLUSIONS

The Abel-Noble equation of state provides a simple analytical relationship that describes the real gas behavior of hydrogen for conventional engineering pressures above ambient (0.1 MPa < P < 200 MPa) and temperatures near ambient (273 K < T < 423 K). The real gas behavior of deuterium is nominally equivalent to hydrogen for the same range of pressure and temperature and tritium is expected to follow the same relationship. This equation of state is appropriate to higher temperature (< 1000 K) for pressures to at least 50 MPa and is probably accurate to pressures of 200 MPa or higher; however, experimental validation is lacking. The Abel-Noble parameter b was determined to be equal to 15.55 $cm^3\ mol^{-1}$ using data previously published for hydrogen.

The fugacity of hydrogen should be used in thermodynamic relationships in place of the pressure. Assuming the Abel-Noble equation of state, the fugacity has a simple analytical form

$$f = P \exp\left(\frac{Pb}{RT}\right) \tag{9}$$

which can easily be incorporated in permeation, diffusion, and solubility calculations. The ratio of fugacity to pressure (often called fugacity coefficient) is about 1.1 at 15 MPa and 298 K, thus even at relatively modest pressures the real behavior of the gas can be important. The fugacity coefficient decreases as temperature increases.

The permeability measurements for austenitic stainless steels that have been reported in the literature are generally quite consistent. These reports show that for single-phase austenitic stainless steels the permeability is independent of the alloy and the microstructure; second phases, such as strain-induced martensite, however, can substantially increase permeation. The relationship of Louthan and Derrick is recommended as a good relationship for extrapolation to ambient temperature [27]. Diffusivity, on the other hand, appears to depend on the alloy; in addition, there may be considerable errors in reported values due to the role of surface condition. The nitrogen-strengthened, high-manganese stainless steels, such as 21Cr-6Ni-9Mn and 22Cr-13Ni-5Mn, for example, have lower diffusivity of hydrogen and higher solubility for hydrogen than the 300-series stainless steels (while the permeability is the same for the two alloy groups).

Since the permeability is essentially the same for all stainless steels, the accuracy of the solubility measured from permeation experiments will depend on the accuracy of the diffusion measurement, which generally has large uncertainty. For stainless steels the total hydrogen concentration in the lattice can be approximated by the lattice solubility since hydrogen is not strongly trapped and equilibrium lattice concentrations are very high. Therefore, hydrogen extraction techniques provide good estimates for solubility. In this report, hydrogen extraction data was used, taking into consideration fugacity, to determine solubility relationships for 304L and 21Cr-6Ni-9Mn. Similar hydrogen extraction data for 316 and 22Cr-13Ni-5Mn correlate well with these relationships for 304L and 21Cr-6Ni-9Mn respectively. These relationships were developed to provide conservatively high solubility when extrapolated to ambient temperature and to account for the pressure and temperature dependence of real gas behavior. Appropriate diffusivity relationships for these two alloy groups can be determined using $D = \Phi / K$. The recommended relationships for permeation, diffusion and solubility are given in Table 8.

V. REFERENCES

1. H Hemmes, A Driessen and R Griessen. Thermodynamic properties of hydrogen at pressures up to 1 Mbar and temperatures between 100 and 1000 K. J Phys C Solid State 19 (1986) 3571-3585.
2. L Zhou and Y Zhou. Determination of compressibility factor and fugacity coefficient of hydrogen in studies of adsorptive storage. Int J Hydrogen Energy 26 (2001) 597-601.
3. KG McLennan and EM Gray. An equation of state for deuterium gas to 1000 bar. Measurement Science and Technology 15 (2004) 211-215.
4. M Tkacz and A Litwiniuk. Useful equations of state of hydrogen and deuterium. J Alloy Compd 330-332 (2002) 89-92.
5. J Peress. Working with Non-Ideal Gases. Chem Eng Prog 99 (2003) 39-41.
6. DR Chenoweth. SAND83-8229 Gas Transfer Analysis: Section H - Real Gas Results via the van der Waals Equation of State and Virial Expansion Extensions of its Limiting Abel-Noble Form. Sandia National Laboratories, (1983).
7. GR Caskey. Hydrogen Effects in Stainless Steels. in: RA Oriani, JP Hirth and M Smialowski, editors. Hydrogen Degradation of Ferrous Alloys. Park Ridge NJ: Noyes Publications (1985) p. 822-862.
8. AD LeClaire. Permeation of Gases Through Solids: 1. Principles. Diffusion and Defect Data 33 (1983) 1-66.

9. AD LeClaire. Permeation of Gases Through Solids: 2. An assessment of measurements of the steady-state permeability of H and its isotopes through Fe, Fe-based alloys, and some commercial steels. Diffusion and Defect Data 34 (1983) 1-35.
10. WG Perkins. Permeation and Outgassing of Vacuum Materials. J Vac Sci Technol 10 (1973) 543-556.
11. J Voelkl and G Alefeld. Hydrogen Diffusion in Metals. in: AS Nowick and JJ Burton, editors. Diffusion in Solids: Recent Developments. New York: Academic Press (1975).
12. MR Louthan and RG Derrick. Permeability of Nickel to High Pressure Hydrogen Isotopes. Scr Metall 10 (1976) 53-55.
13. NR Quick and HH Johnson. Permeation and Diffusion of Hydrogen and Deuterium in 310 Stainless Steel, 472K to 779K. Metall Trans 10A (1979) 67-70.
14. WA Swansiger and R Bastasz. Tritium and Deuterium Permeation in Stainless Steels: Influence of Thin Oxide Films. J Nucl Mater 85 & 86 (1979) 335-339.
15. KS Forcey, DK Ross, JCB Simpson and DS Evans. Hydrogen Transport and Solubility in 316L and 1.4914 Steels for Fusion Reactor Applications. J Nucl Mater 160 (1988) 117-124.
16. T Shiraishi, M Nishikawa, T Tamaguchi and K Kenmotsu. Permeation of mulit-component hydrogen isotopes through austenitc stainless steels. J Nucl Mater 273 (1999) 60-65.
17. A Michels, W De Graff, T Wassenaar, JMH Levelt and L P. Compressibility Isotherms of Hydrogen and Deuterium at Temperatures between -175˚C and +150˚C (at Densities up to 960 Amagat). Physica 25 (1959) 25-42.
18. NB Vargaftik. Tables on the Thermophysical Properties of Liquids and Gases: in Normal and Dissociated States. London: Hemisphere Publishing Corporation (1975).
19. AS Zarchy and RC Axtmann. Tritium permeation through 304 stainless steel at ultra-low pressures. J Nucl Mater 79 (1979) 110-117.
20. GR Caskey. Hydrogen Solution in Stainless Steels (DPST-83-425). Savannah River Laboratory, Aiken SC (May 1983).
21. RA Oriani. Hydrogen embrittlement of steels. Ann Rev Mater Sci 8 (1978) 327-357.
22. HP van Leeuwen. Fugacity of Gaseous Hydrogen. in: RA Oriani, JP Hirth and M Smialowski, editors. Hydrogen Degradation of Ferrous Alloys. Park Ridge NJ: Noyes Publications (1985) p. 16-35.
23. RA Oriani. The Physical and Metallurigical Aspects of Hydrogen in Metals. Fusion Technology 26 (1994) 235-66.
24. VV Fedorov, VI Pokhmursky, EV Dyomina, MD Prusakova and NA Vinogradova. Hydrogen permeability of austenitic steels proposed for fusion reactor first wall. Fusion Technology 28 (1995) 1153-1158.
25. RA Strehlow and HC Savage. Formation and use of oxide films to impede outgassing of metals. J Nucl Mater 53 (1974) 323-327.
26. WA Swansiger, RG Musket, LJ Weirick and W Bauer. Deuterium permeation through 309S stainless steel with thin, characterized oxides. J Nucl Mater 53 (1974) 307-312.
27. MR Louthan and RG Derrick. Hydrogen Transport in Austenitic Stainless Steel. Corros Sci 15 (1975) 565-577.
28. GR Caskey and RD Sisson. Hydrogen Solubility in Austenitic Stainless Steels. Scr Metall 15 (1981) 1187-1190.
29. XK Sun, J Xu and YY Li. Hydrogen Permeation Behaviour in Austenitic Stainless Steels. Mater Sci Eng A114 (1989) 179-187. (these authors have also been referenced as Sun Xuikui, Xu Jian, Li Yiyi)

30. T-P Perng and CJ Altstetter. Effects of Deformation on Hydrogen Permeation in Austenitic Stainless Steels. Acta metall 34 (1986) 1771-1781.
31. XK Sun, J Xu and YY Li. Hydrogen permeation behavior in metastable austenitic stainless steels 321 and 304. Acta metall 37 (1989) 2171-2176. (these authors have also been referenced as Sun Xuikui, Xu Jian, Li Yiyi)
32. AI Gromov and YK Kovneristyi. Permeability, Diffusion, and Solubility of Hydrogen in Cr-Ni and Cr-Mn Austenitic Steels. Met Sci Heat Treat 22 (1980) 321-324. (data from XK Sun, J Xu and YY Li. Hydrogen Permeation Behaviour in Austenitic Stainless Steels. Mater Sci Eng A114 (1989) 179-187.)
33. EH VanDeventer and VA Maroni. Hydrogen Permeation Characteristics of some Austenitic and Nickel-base Alloys. J Nucl Mater 92 (1980) 103-111.
34. T Tanabe, Y Tamanishi, K Sawada and S Imoto. Hydrogen Transport in Stainless Steels. J Nucl Mater 122&123 (1984) 1568-1572.
35. E Hashimoto and T Kino. Hydrogen Permeation Through Type 316 Stainless Steels and Ferritic Steel for Fusion Reactor. J Nucl Mater 133&134 (1985) 289-291.
36. DM Grant, DL Cummings and DA Blackburn. Hydrogen in 316 Steel - Diffusion, Permeation and Surface Reaction. J Nucl Mater 152 (1988) 139-145.
37. MR Louthan, GR Caskey, JA Donovan and DE Rawl. Hydrogen Embrittlement of Metals. Mater Sci Eng 10 (1972) 357-368.
38. J Xu, XK Sun, WX Chen and YY Li. Hydrogen Permeation and Diffusion in Iron-base Superalloys. Acta metall mater 41 (1993) 1455-1459.
39. L Ma, G Liang, J Tan, L Rong and Y Li. Effect of Hydrogen on Cryogenic Mechanical Properties of Cr-Ni-Mn-N Austenitic Steels. J Mater Sci Technol 15 (1999) 67-70.
40. LM Ma, GJ Liang and YY Li. Effect of Hydrogen Charging on Ambient and Cryogenic Mechanical Properties of a Precipitate-Strengthened Austenitic Steel. in: FR Fickett and RP Reed, editors. Proceedings of the International Cryogenic Materials Conference, 1991, Huntsville AL. Advances in Cryogenic Engineering, vol. 38A. Plenum Press, NY (1992) p. 77-84.

APPENDIX A. Units

The units that are used for permeability and solubility of hydrogen vary substantially in the literature, often leading to confusion. Solubility units are a measure of concentration normalized by the square root of pressure. Permeability units are more difficult to visualize: flux normalized by a characteristic distance (thickness) and the square root of pressure. The flux is concentration per time per surface area. The concentration unit varies according to the motivation of the disciple making use of the information. For relatively low concentrations of interstitial atoms, the metallurgist prefers parts per million (ppm) and to complicate matters, two variants are commonly used: atomic ppm and weight ppm. Systems engineers, on the other hand, prefer standard gas volumes (cubic centimeters or liters) per volume of material. Others in the scientific community have settled on moles of H_2 gas per volume (cubic meter) of material. It must be kept in mind when converting between these units that two atoms make a molecule of hydrogen gas, but when dissolved in the lattice of a metal the hydrogen exists as atomic hydrogen, therefore a factor of two is necessary when converting between atoms of hydrogen dissolved in the material

and the equivalent amount of hydrogen gas. In addition, gas equivalence requires a standard reference state, standard temperature and pressure, but in practice there is no universal definition of standard temperature and pressure. When not stated we assume standard temperature and pressure to be 273 K and 0.101325 MPa. Older studies typically used atmospheres for pressure units, but recent studies have settled in on the megapascal (MPa). The recommended units for solubility and permeability are then

$$\frac{\text{mol } H_2}{m^3 \cdot MPa^{1/2}} \qquad \text{solubility}$$

$$\frac{\text{mol } H_2}{m \cdot s \cdot MPa^{1/2}} \qquad \text{permeability}$$

Table A provides conversion factors for a number of commonly reported units.

There are several inconsistencies in the data reported by Caskey. The pressure units reported in Ref. [7] for permeability and solubility are believed to be incorrect; $\sqrt{MPa}$ should be replaced with $\sqrt{atm}$ (i.e., the values reported by Caskey have units of mol m^{-1} s^{-1} $atm^{-1/2}$ and mol m^{-3} $atm^{-1/2}$ for permeability and solubility respectively). In Ref. [20], Caskey quotes hydrogen precharging temperature as 740 K, while plots seems to indicate that then temperature was in fact 470 K as described in another reference [28].

Table 1. Permeability, diffusivity and solubility relationships: average values determined for several austenitic stainless steels.

Alloy	Temperature Range (K)	Pressure Range (MPa)	Permeability $\Phi = \Phi_o \exp(-H_\Phi / RT)$		Diffusivity $D = D_o \exp(-H_D / RT)$		Solubility $K = K_o \exp(-\Delta H_s / RT)$		Ref.
			Φ_o $\left(\frac{\text{mol H}_2}{\text{m}\cdot\text{s}\cdot\sqrt{\text{MPa}}}\right)$	H_Φ $\left(\frac{\text{kJ}}{\text{mol}}\right)$	D_o $\left(\frac{\text{m}^2}{\text{s}}\right)$	H_D $\left(\frac{\text{kJ}}{\text{mol}}\right)$	K_o $\left(\frac{\text{mol H}_2}{\text{m}^3\cdot\sqrt{\text{MPa}}}\right)$	ΔH_s $\left(\frac{\text{kJ}}{\text{mol}}\right)$	
Average of several alloys	423-700	0.1-0.3	1.2×10^{-4}	59.8	6.6×10^{-7}	54.0	179	5.9	[27] [a]
Average of six alloys	473-703	0.1	2.81×10^{-4}	62.27	5.76×10^{-7}	53.62	488	8.65	[29]
Based on >20 studies on 12 austenitic alloys	—	—	3.27×10^{-4}	65.69	—	—	—	—	[9]
Average of four alloys (301, 302, 304, 310)	373-623	1×10^{-4} -0.03	0.535×10^{-4}	56.1	2.01×10^{-7}	49.3	266	6.86	[30]
304L	Determined from hydrogen extraction techniques						203	7.5	[20]
21-6-9							345	7.5	[20]
304L							135	5.9	This study
21-6-9							222	5.9	This study
A-286 / JBK-75 aged							104	5.9	This study

[a] from deuterium data: permeability and diffusivity corrected to hydrogen by multiplying by the square root of the mass ratio: $\sqrt{2}$.

Table 2. Measured hydrogen concentration after thermal precharging stainless steels in high-pressure hydrogen gas; all precharging performed at 197˚C. Data from [28].

Material	Measured [H] (ppm)	Precharging Pressure (MPa)	Fugacity (MPa)	Solubility $\left(\frac{\text{mol } H_2}{m^3 \cdot \sqrt{MPa}}\right)$
304L annealed	72	69	91	29.6
304L annealed, EP	81	69	91	33.3
304L CW	71	69	91	29.2
304L CW, EP	81	69	91	33.3
304L HERF	71	69	91	29.2
304L HERF, EP	79	69	91	32.4
			Average ± standard deviation	31.1 ± 2
21-6-9 annealed	118	69	91	48.5
21-6-9 annealed, EP	126	69	91	51.7
21-6-9 CW	126	69	91	51.7
21-6-9 CW, EP	127	69	91	52.2
21-6-9 HERF	119	69	91	48.9
21-6-9 HERF, EP	126	69	91	51.7
			Average ± standard deviation	50.8 ± 2
modified A-286 annealed	80	69	91	33.0
modified A-286 annealed, EP	81	69	91	33.4
modified A-286 HERF	51	69	91	21.0
modified A-286 HERF, EP	55	69	91	22.7
			Average, all	27.5
			Average, annealed	33.2
			Average, HERF	21.9

EP = electropolished, CW = cold-worked, HERF = high energy rate forged

Table 3. Measured hydrogen concentration after thermal precharging 304 stainless steels in high-pressure hydrogen gas; all precharging performed at 300˚C.

Material	Measured [H] (ppm)	Precharging Pressure (MPa)	Fugacity (MPa)	Solubility $\left(\frac{\text{mol } H_2}{m^3 \cdot \sqrt{MPa}}\right)$
304L annealed	62	34	38.6	39.1
304L	140	138	216	37.3
304L LENS	140	138	216	37.3
304L annealed	37	7	7.1	54.5
304L forged	150	138	216	39.9
304L annealed	130	138	216	34.6
304 base	130	138	216	34.6
304 base	130	138	216	34.6
304/308 weld	130	138	216	34.6
304/308 weld	130	138	216	34.6
			Average ± standard deviation	38.1 ± 6

Table 4. Measured hydrogen concentration after thermal precharging 316 stainless steels in high-pressure hydrogen gas; all precharging performed at 300˚C.

Material	Measured [H] (ppm)	Precharging Pressure (MPa)	Fugacity (MPa)	Solubility $\left(\frac{\text{mol } H_2}{m^3 \cdot \sqrt{MPa}}\right)$
316 heat 1, CW	140	138	216	37.5
316 heat 1, annealed	140	138	216	37.5
316 heat 1, CW	140	138	216	37.5
316 heat 1, annealed	140	138	216	37.5
316 heat 4, CW	130	138	216	34.8
316 heat 4, CW	130	138	216	34.8
316 heat 1, CW	150 [a]	138	216	40.2
316 heat 1, annealed	140 [a]	138	216	37.5
316 heat 4, CW	130 [a]	138	216	34.8
316 heat 1, CW	140	138	216	37.5
316 heat 2, CW	130	138	216	34.8
316 heat 4, CW	120	138	216	32.1
			Average ± standard deviation	36.4 ± 2

CW = cold-worked

[a] repeated analysis on material stored at –20˚C for 8 months

Table 5. Measured hydrogen concentration after thermal precharging 21-6-9 stainless steels in high-pressure hydrogen gas; all precharging performed at 300˚C.

Material	Measured [H] (ppm)	Precharging Pressure (MPa)	Fugacity (MPa)	Solubility $\left(\frac{\text{mol } H_2}{m^3 \cdot \sqrt{MPa}}\right)$
21-6-9 HERF	270	138	216	71.3
21-6-9 forging	270	138	216	71.3
21-6-9 HERF	280	138	216	73.9
21-6-9 HERF	280	138	216	73.9
21-6-9 forging	270	138	216	71.3
21-6-9 forging	280	138	216	73.9
21-6-9 forging	280	138	216	73.9
21-6-9 forging	200	138	216	52.8
21-6-9 forging	210	138	216	55.5
21-6-9 annealed	230	138	216	60.7
21-6-9 annealed	230	138	216	60.7
21-6-9 weld	230	138	216	60.7
21-6-9 annealed	230	138	216	60.7
21-6-9 annealed	240	138	216	63.4
21-6-9 base	210	138	216	55.5
21-6-9 base	210	138	216	55.5
21-6-9 forging, FN~0	230	138	216	60.7
21-6-9 forging, FN~2	220	138	216	58.1
21-6-9 plate/bar	190	138	216	50.2
21-6-9/308 weld	150 [a]	138	216	39.6
21-6-9/308 weld	150 [a]	138	216	39.6
			Average ± standard deviation	63.4 ± 8
21-6-9, Ref. [39]	65	10	10.3	78.5

FN = ferrite number, determined with magnetic gauge

[a] not included in average

Table 6. Measured hydrogen concentration after thermal precharging 22-13-5 stainless steels in high-pressure hydrogen gas; all precharging performed at 300˚C.

Material	Measured [H] (ppm)	Precharging Pressure (MPa)	Fugacity (MPa)	Solubility $\left(\frac{\text{mol } H_2}{m^3 \cdot \sqrt{MPa}}\right)$
22-13-5 annealed	140	69	86.3	59.0
22-13-5 heat 1, SHT	140	69	86.3	59.0
22-13-5 heat 2, SHT	140	69	86.3	59.0
22-13-5 bar	120	69	86.3	50.5
22-13-5 HERF (770[a])	240	138	216	63.9
22-13-5 HERF (650[a])	250	138	216	66.5
22-13-5 forging	230	138	216	61.2
22-13-5 HERF (770[a])	200	138	216	53.2
22-13-5 HERF (650[a])	180	138	216	47.9
			Average ± standard deviation	57.8 ± 6

[a] yield strength (MPa)

SHT = solution heat treated, HERF = high energy rate forged

Table 7. Measured hydrogen concentration after thermal precharging A-286 and JBK-75 stainless steels in high-pressure hydrogen gas; all precharging performed at 300˚C.

Material	Measured [H] (ppm)	Precharging Pressure (MPa)	Fugacity (MPa)	Solubility $\left(\frac{\text{mol } H_2}{m^3 \cdot \sqrt{MPa}}\right)$
JBK-75	110	138	216	29.4
JBK-75	110	138	216	29.4
A-286 heat 1	120	138	216	32.1
A-286 heat 1, re-aged	120	138	216	32.1
A-286 heat 2	110	138	216	29.4
			Average ± standard deviation	30.5 ± 1
JBK-75, Ref. [40]	25	10	10.3	30.6

Table 8. Recommended permeability, diffusivity and solubility relationships for austenitic stainless steels.

Alloy	Permeability $\Phi = \Phi_o \exp(-H_\Phi / RT)$		Diffusivity $D = D_o \exp(-H_D / RT)$		Solubility $K = K_o \exp(-\Delta H_s / RT)$		Ref.
	Φ_o $\left(\frac{\text{mol H}_2}{\text{m} \cdot \text{s} \cdot \sqrt{\text{MPa}}}\right)$	H_Φ $\left(\frac{\text{kJ}}{\text{mol}}\right)$	D_o $\left(\frac{\text{m}^2}{\text{s}}\right)$	H_D $\left(\frac{\text{kJ}}{\text{mol}}\right)$	K_o $\left(\frac{\text{mol H}_2}{\text{m}^3 \cdot \sqrt{\text{MPa}}}\right)$	ΔH_s $\left(\frac{\text{kJ}}{\text{mol}}\right)$	
All austenitic stainless steels	1.2×10^{-4}	59.8	—	—	—	—	[27]
300-series	—	—	8.9×10^{-7}	53.9	135	5.9	This study
21Cr-6Ni-9Mn 22Cr-13Ni-5Mn	—	—	5.4×10^{-7}	53.9	222	5.9	This study
A-286 / JBK-75 aged	—	—	1.2×10^{-6}	53.9	104	5.9	This study

Table A. Unit conversions for quantities commonly encountered in permeability, diffusivity and solubility studies. Note that a number of conversions require knowledge of the physical properties of the material (density, molecular weight) or a clear definition of the standard state chosen for the gas, therefore some of the conversion below are not universal.

To convert from	To	Multiply by
atm	MPa	0.101325
mol H_2	g	2.016
mol H_2	cm^3	22414 [a]
Energy		
eV	kJ mol^{-1}	96.486
cal mol^{-1}	kJ mol^{-1}	4.184
Solubility		
$\frac{\text{mol } H_2}{m^3 \cdot atm^{1/2}}$	$\frac{\text{mol } H_2}{m^3 \cdot MPa^{1/2}}$	3.14153
$\frac{cm^3}{cm^3 \cdot atm^{1/2}}$	$\frac{\text{mol } H_2}{m^3 \cdot MPa^{1/2}}$	140.16 [a]
$\frac{\text{g H}}{g \cdot MPa^{1/2}}$	$\frac{\text{mol } H_2}{m^3 \cdot MPa^{1/2}}$	3.9×10^6 [b]
$\frac{\text{wt ppm H}}{MPa^{1/2}}$	$\frac{\text{mol } H_2}{m^3 \cdot MPa^{1/2}}$	3.9 [b]
$\frac{\text{at ppm H}}{MPa^{1/2}}$	$\frac{\text{mol } H_2}{m^3 \cdot MPa^{1/2}}$	0.0718 [b,c]
Diffusivity		
$cm^2\ s^{-1}$	$m^2\ s^{-1}$	0.0001
Permeability		
$\frac{\text{mol } H_2}{m \cdot s \cdot atm^{1/2}}$	$\frac{\text{mol } H_2}{m \cdot s \cdot MPa^{1/2}}$	3.14153
$\frac{cm^3}{cm \cdot s \cdot atm^{1/2}}$	$\frac{\text{mol } H_2}{m \cdot s \cdot MPa^{1/2}}$	0.014016 [a]
$\frac{\text{mol } H_2}{m^3 \cdot MPa^{1/2}}$	$\frac{\text{mol } H_2}{m^3 \cdot MPa^{1/2}}$	
$\frac{\text{mol } H_2}{m^3 \cdot atm^{1/2}}$	$\frac{\text{mol } H_2}{m^3 \cdot MPa^{1/2}}$	3.14153

[a] at STP, standard pressure and temperature: P = 0.101325 MPa, T = 273.15 K

[b] assumes density of solid to be 7.9 g cm^{-3} (stainless steel), and limit of small H content

[c] assumes equivalent molecular weight of solid to be 55 g mol^{-1} (stainless steel) , and limit of small H content

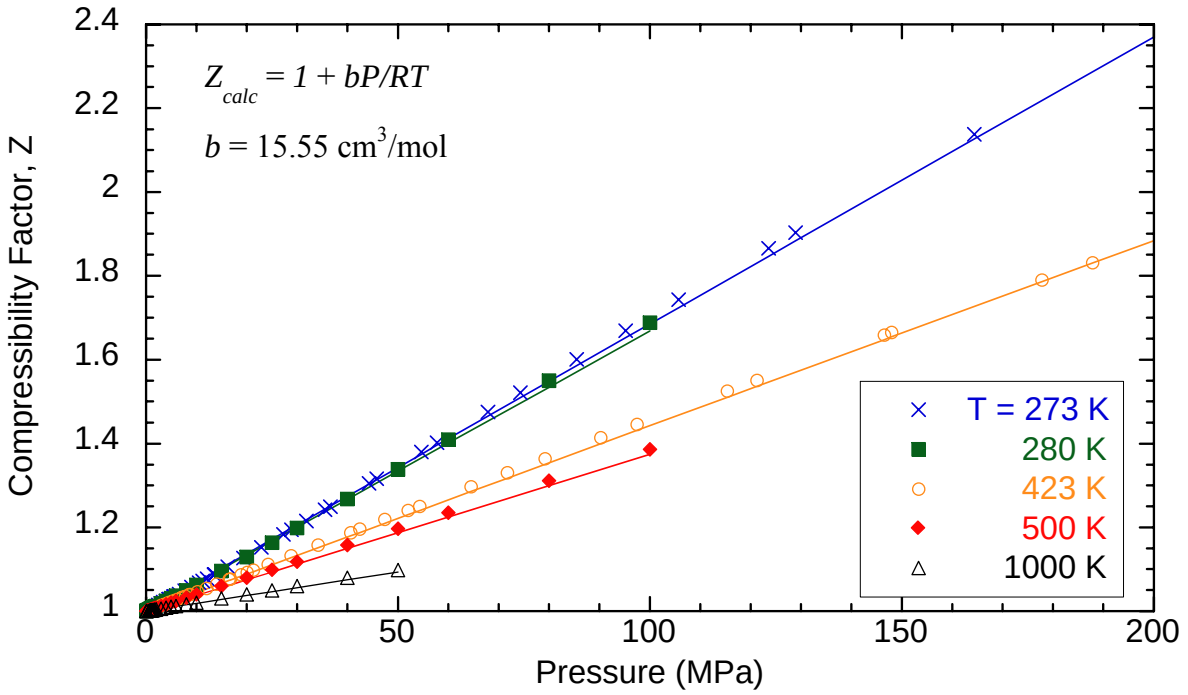

Figure 1. Compressibility factor as a function of pressure and temperature. Lines are calculated using the Abel-Noble equation of state, and the symbols represent data from Refs. [17, 18].

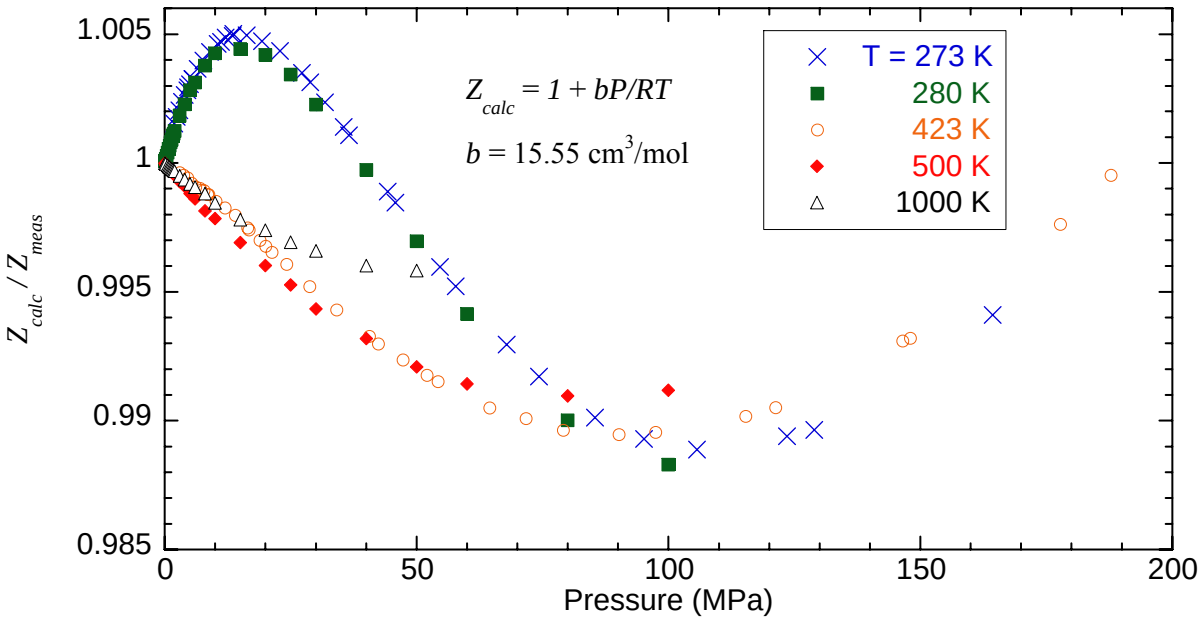

Figure 2. The ratio of the calculated to the measured compressibility factor using data from Figure 1.

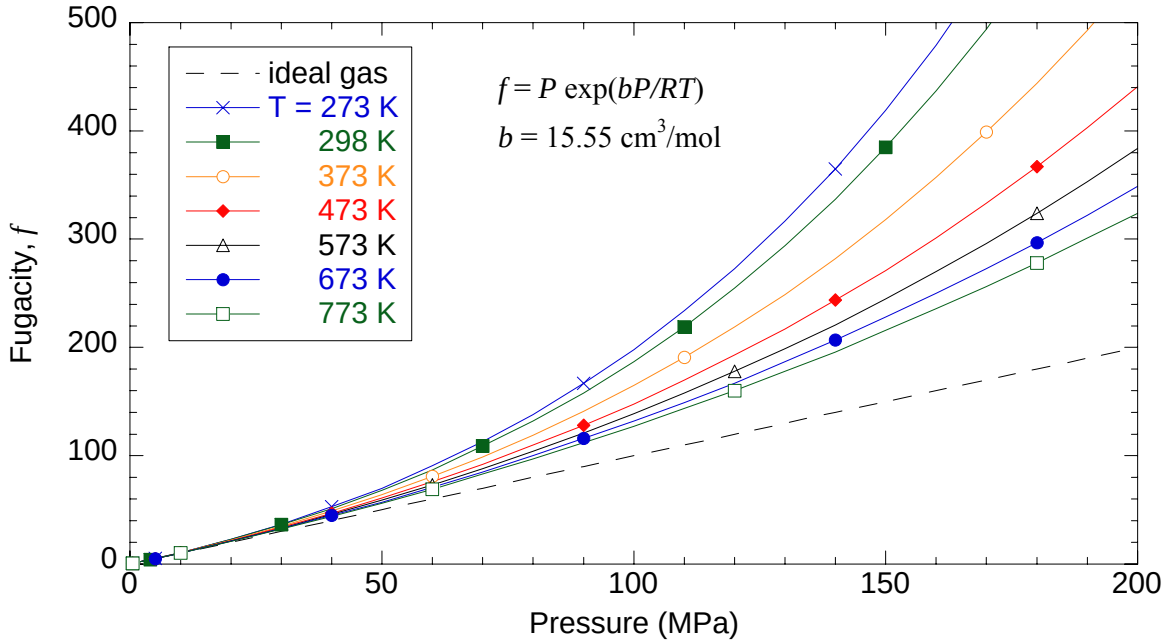

Figure 3. Fugacity as a function of pressure using the Abel-Noble equation of state.

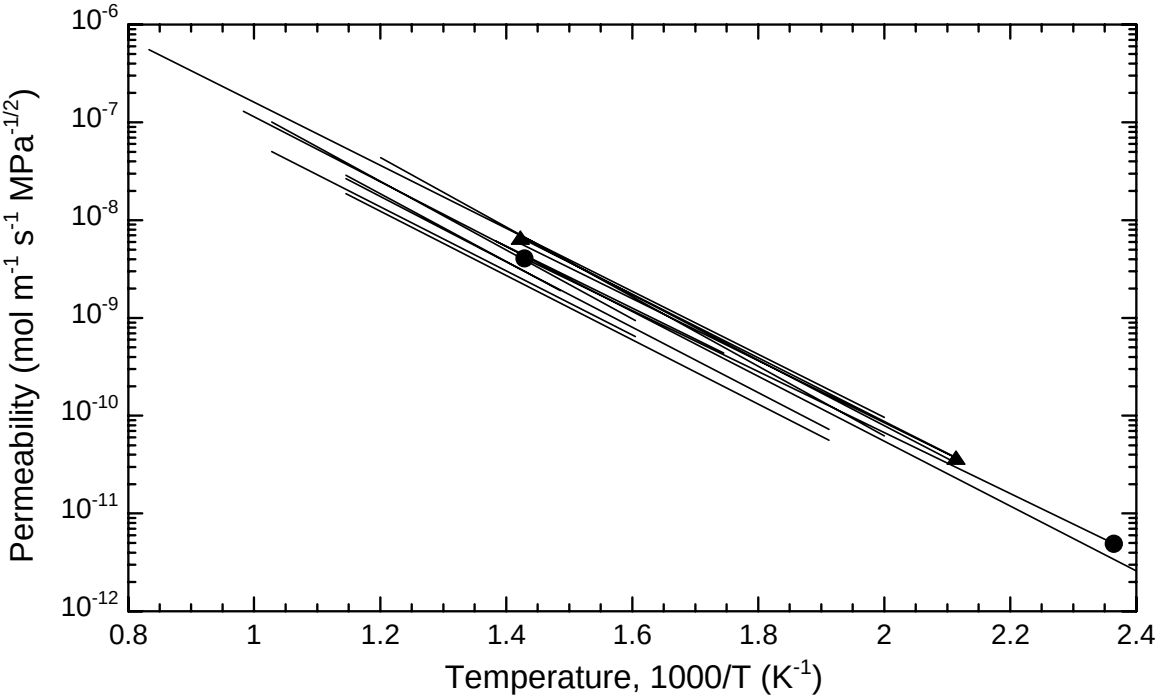

Figure 4. Permeability of 316 stainless steel alloys. Circles: average of several different austenitic stainless steels [27]. Triangles: average of six austenitic stainless steels [29]. Other full lines: [15, 16, 32-36].

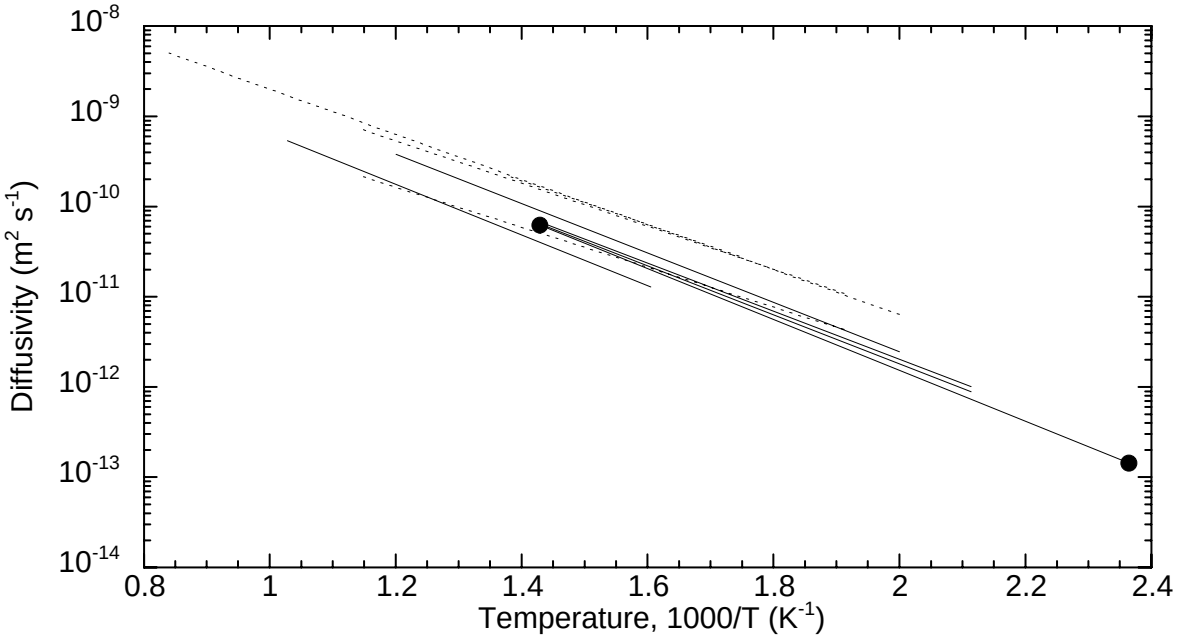

Figure 5. Diffusivity of 316 stainless steel alloys. Circles: average for several different austenitic stainless steels [27]. Full lines: [29, 32, 36]. Dotted lines represent relationships from studies that feature low solubility, same studies dotted in Figure 6 [15, 34, 35].

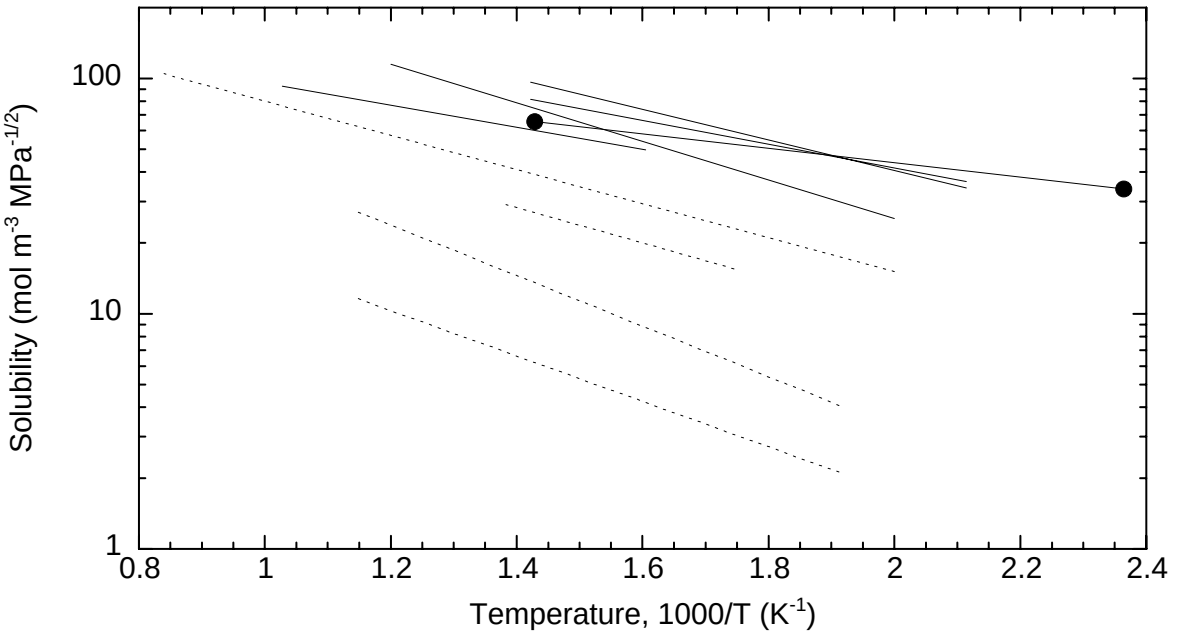

Figure 6. Solubility of 316 stainless steel alloys. Circles: average of several austenitic stainless steels [27]. Full lines: [29, 32, 36]. Dotted lines represent relationships that display low solubility [15, 16, 34, 35], same studies dotted in Figure 5.

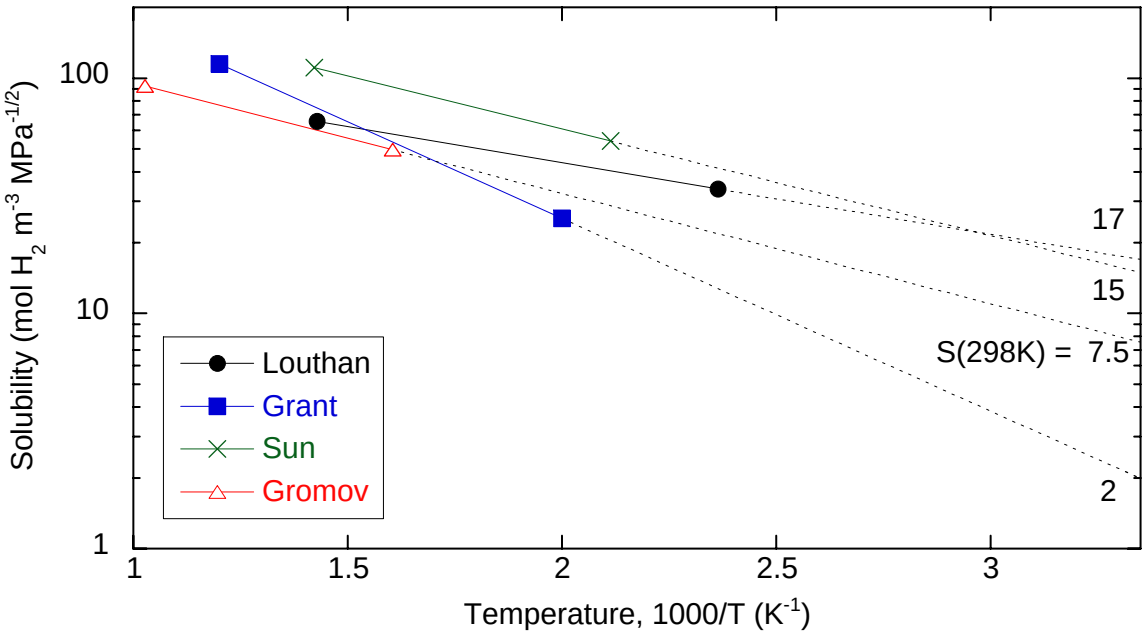

Figure 7. Solubility of hydrogen in austenitic stainless steels from several studies extrapolated to ambient temperature: Louthan [27] and Sun [29], average from several austenitic stainless steels; Gromov [32], 316L; and Grant [36], 316.

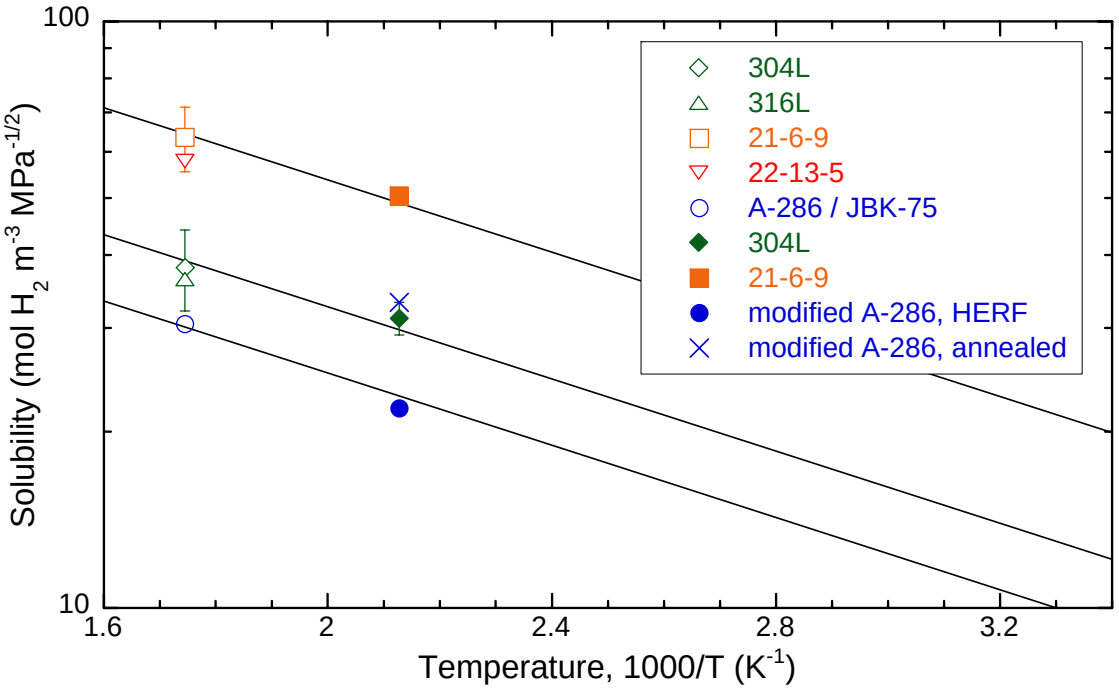

Figure 8. Solubility fit to hydrogen extraction data: open symbols, data from Tables 3-7, closed symbols, data from Table 2 and Refs. [20, 28].